Atmospheric Environment 45 (2011) 3352–3359

Contents lists available at ScienceDirect

Atmospheric Environment

journal homepage: www.elsevier.com/locate/atmosenv

Effect of real-time boundary wind conditions on the air flow and pollutant dispersion in an urban street canyon—Large eddy simulations

Yun-Wei Zhang [a], Zhao-Lin Gu [b,c,*], Yan Cheng [b], Shun-Cheng Lee [d]

[a] School of Energy and Power Engineering, Xi'an Jiaotong University, Xi'an 710049, China
[b] School of Human Settlements and Civil Engineering, Xi'an Jiaotong University, Xi'an 710049, China
[c] SKLLQG, Institute of Earth Environment, Chinese Academy of Sciences, China
[d] Department of Civil and Structural Engineering, The Hong Kong Polytechnic University, Hung Hom, Kowloon, Hong Kong, China

ARTICLE INFO

Article history:
Received 27 December 2010
Received in revised form
24 March 2011
Accepted 24 March 2011

Keywords:
Street canyon
Boundary condition
Air flow
Pollutant dispersion
Large eddy simulation

ABSTRACT

Air flow and pollutant dispersion characteristics in an urban street canyon are studied under the real-time boundary conditions. A new scheme for realizing real-time boundary conditions in simulations is proposed, to keep the upper boundary wind conditions consistent with the measured time series of wind data. The air flow structure and its evolution under real-time boundary wind conditions are simulated by using this new scheme. The induced effect of time series of ambient wind conditions on the flow structures inside and above the street canyon is investigated. The flow shows an obvious intermittent feature in the street canyon and the flapping of the shear layer forms near the roof layer under real-time wind conditions, resulting in the expansion or compression of the air mass in the canyon. The simulations of pollutant dispersion show that the pollutants inside and above the street canyon are transported by different dispersion mechanisms, relying on the time series of air flow structures. Large scale air movements in the processes of the air mass expansion or compression in the canyon exhibit obvious effects on pollutant dispersion. The simulations of pollutant dispersion also show that the transport of pollutants from the canyon to the upper air flow is dominated by the shear layer turbulence near the roof level and the expansion or compression of the air mass in street canyon under real-time boundary wind conditions. Especially, the expansion of the air mass, which features the large scale air movement of the air mass, makes more contribution to the pollutant dispersion in this study. Comparisons of simulated results under different boundary wind conditions indicate that real-time boundary wind conditions produces better condition for pollutant dispersion than the artificially-designed steady boundary wind conditions.

1. Introduction

High pollutant concentrations in urban street canyons do create health impacts to people (Fenger, 1999; WHO, 2006; Cooke et al., 2007). It is, therefore, important to understand the dispersion characteristics of pollutants in street canyons under real urban meteorological conditions, to formulate effective strategies for emission control and urban planning.

Several methods, such as wind-tunnel experiments (Klein and Plate, 1999; Pavageau and Schatzmann, 1999; Baik et al., 2000; Gromke and Ruck, 2007), field measurements (Depaul and Sheih, 1985; Rotach, 1995; Eliasson et al., 2006) computational fluid dynamics (CFD) simulations (Walton and Cheng, 2002; Cai et al., 2008; Yang and Shao, 2008; Li et al., 2009), have been used to investigate the air flow and pollutant dispersion in urban street canyons. As commonly known, the air flow structure and strength in a street canyon are related to upper boundary wind conditions (Vardoulakis et al., 2003). Field measurements and wind-tunnel experiments have shown that canyon flows are characterized by an intermittent vortex inside the canyon and a shear layer at the roof level (Rotach, 1995; Klein and Plate, 1999; Louka et al., 2000) when boundary air flows are approximately at a perpendicular incidence to the street. Effects of high aspect ratio (AR) of the street (Eliasson et al., 2006; Li et al., 2009; Murena et al., 2009; Zhang et al., 2011), thermal condition inside the street canyon (Kim and Baik, 2001), and tree plantings on the street ground surface (Gromke and Ruck, 2007; Gu et al., 2010) have also been investigated when boundary air flows are perpendicular to the street. When boundary air flows are at an arbitrary incidence to the street, the induced canyon flows

* Corresponding author. School of Human Settlements and Civil Engineering, Xi'an Jiaotong University, Xi'an 710049, China. Tel./fax: +86 29 8339 5100.
E-mail address: guzhaoln@mail.xjtu.edu.cn (Z.-L. Gu).

1352-2310/$ – see front matter © 2011 Elsevier Ltd. All rights reserved.
doi:10.1016/j.atmosenv.2011.03.055

can be divided into regimes of channel flow along the aisles and of wake flow in the canyons (Yang and Shao, 2008).

It is known that the time-averaged wind velocity and direction show considerable diurnal changes in field measurements (Louka et al., 2000). The variations of wind velocity and direction can still be observed even when measurement data are logged at frequencies higher than 10 Hz (Walton et al., 2002). It is anticipated that the turbulence of canyon flow and the pollutant dispersion show diurnal changes as well. Almost all previous studies by wind-tunnel experiments and CFD simulations are based on the steady boundary-wind conditions (SBC). Only the mean wind velocity and the prevailing wind direction are used in CFD simulations for the boundary wind conditions (Klein and Plate, 1999; Yang and Shao, 2008; Gu et al., 2010). However, the temporal variations of the ambient wind velocity and direction make a time series of boundary conditions and lead to the induced canyon flow more turbulent than that under SBC, especially under the weak wind condition (mean ambient wind velocity $< 1.5\ \mathrm{m\,s^{-1}}$) (Vardoulakis et al., 2003). Studies have revealed that the removal of pollutants from the canyon to upper air flow is dominated by turbulent processes (Hoydysh and Dabberdt, 1988; Walton and Cheng, 2002; Li et al., 2009). These turbulent processes are commonly referred to as the Kelvin–Helmholtz instability, or the flapping of the shear layer at the roof level (Louka et al., 2000).

The flapping of the shear layer results in the highly intermittent flow behavior inside the street canyon, as found in experiments (Louka et al., 2000). The shear layer is generated due to the differences between the air flow velocities in and above the street canyon. The time series of boundary wind conditions might be an important factor influencing the strength and the flapping of the shear layer. Based on SBC, the simulated air flow within the street canyon is found to be in roughly constant vortex structure and strength, which might not fully reveal the variations of the strength and vertical position of the shear layer (Liu and Barth, 2002; Cui et al., 2004; Zhang et al., 2011). Inside the street canyon, instantaneous fluctuation of the wind velocity under real-time boundary wind conditions (RTBC) should be stronger than the mean recirculation of air flow (Louka et al., 2000). Therefore, how to set RTBC in simulations is of vital importance in grasping the characteristics of the instantaneous air flows and pollutant dispersion in urban street canyons.

In this study, the air flow and pollutant dispersion inside a street canyon is simulated with a large eddy simulation (LES) turbulence model. The novelty of this work is the simulation of air flow structure evolutions inside and above the street canyon under temporally varied ambient wind conditions. Especially, a scheme for realizing the RTBC in simulations is proposed to show the effects of RTBC on the induced canyon flow theoretically. Instantaneous and statistical air flow structures and pollutant dispersion processes inside and above the street canyon are investigated to demonstrate the evolution of the street canyon air flow and the transport processes of pollutants from the canyon to the upper air layer.

2. Numerical model formations

2.1. Large eddy simulation equations

LES is used to simulate air flow and turbulence distributions, assuming the incompressibility of air mass. By applying the top-hat (box) filter to Navier–Stokes equations, the governing equation for LES are obtained in the form of continuity equation

$$\frac{\partial \overline{u_i}}{\partial x_i} = 0 \tag{1}$$

and the momentum equations

$$\frac{\partial \overline{u_i}}{\partial t} + \frac{\partial\left(\overline{u_i}\overline{u_j}\right)}{\partial x_j} = -\frac{\partial \overline{p}}{\partial x_i} - \frac{\partial \tau_{ij}}{\partial x_j} + \frac{1}{\mathrm{Re}}\frac{\partial^2 \overline{u_i}}{\partial x_j \partial x_j} + S_i \tag{2}$$

where $\overline{u}_i$ and $\overline{u}_j$ are resolved-scale velocities in i and j directions, $\overline{p}$ is the resolved-scale virtual pressure, $\tau_{ij} = -2\nu_{\mathrm{sgs}}\overline{S}_{ij} + \frac{1}{3}\tau_{kk}\delta_{ij}$, is the subgrid-scale stress (SGS), and S_i is the additional source term, which contains all the other terms not explicitly appearing in these equations (Tao, 2005). Subgrid-scale viscosity is calculated by $\nu_{\mathrm{sgs}} = (C_s)^2(C_L\overline{\Delta})^2|\overline{S}|$. Where, C_s is the Smagorinsky model constant (Smagorinsky, 1963), C_L is the modification coefficient for the SGS characteristic length. The detailed computational process was reported by Qiu et al. (2008).

Pollutant dispersion is simulated by the scalar transport equation

$$\frac{\partial \overline{c}}{\partial t} + \frac{\partial\left(\overline{u_j c}\right)}{\partial x_j} = \frac{\partial}{\partial x_j}\left[\left(\frac{\nu + \nu_{SGS}}{Sc}\right)\frac{\partial \overline{c}}{\partial x_j}\right] + S_0 \tag{3}$$

where $\overline{c}$ is the resolved pollutant concentration, Sc is the Schmidt number and S_0 is the pollutant source emission. Equations (1)–(3) are expressed in tensor notation so that the indices i and j range within values (1, 2, 3), corresponding to (x, y, z) directions in space.

2.2. Boundary conditions

Simulations are performed on an idealized, infinitely long symmetric street canyon model of AR = 1 (canyon width (W)/building height (H)). To reduce the computational load and account for the consequence of air flow in a long street, periodic boundary conditions (PBC) are adopted for the specified street canyon length (L=2H) in the spanwise direction. PBC are also adopted in the streamwise (x) direction to demonstrate the consequences of air flows in a series of canyons. The upper boundary is specified as a slip condition with zero vertical variation. Wall functions are resorted to for the determination of wind velocities near all solid walls, as illustrated by Walton et al. (2002). A non-uniform grid system is used, with a minimum grid width of 0.008H in the x and z directions near the building walls (Walton and Cheng, 2002). According to former studies, the selection of the computational domain and the grid system should be appropriate to show the air flow structures inside and above the street canyons numerically (Walton and Cheng, 2002; Cui et al., 2004; Li et al., 2008). Vehicle emission sources are treated as two line sources near the road surface in the simulation, as shown in Fig. 1(a).

2.3. Numerical method

A self-developed software, which has been validated in our previous work (Gu et al., 2010), is used to solve the governing equations. A scheme, which is described in details in section 3 is used to realize RTBC above the roof level in the current simulation.

3. A scheme for realizing real-time upper boundary wind conditions

Given upper boundary (above the roof level) wind conditions, PBC that feedback the outlet velocities to the inlet boundary at every time step, are usually used in simulations to allow the air flow in the street canyon to gradually develop into a steady flow profile (Walton and Cheng, 2002). Based on PBC, flow profiles can be adjusted as well by adding dynamic pressure drops between the inlet and outlet boundaries (Qiu et al., 2008; Zhang et al., 2011). As a consequence of real-time or stochastic upper wind conditions, the air flow in the street canyon is a non-steady flow.

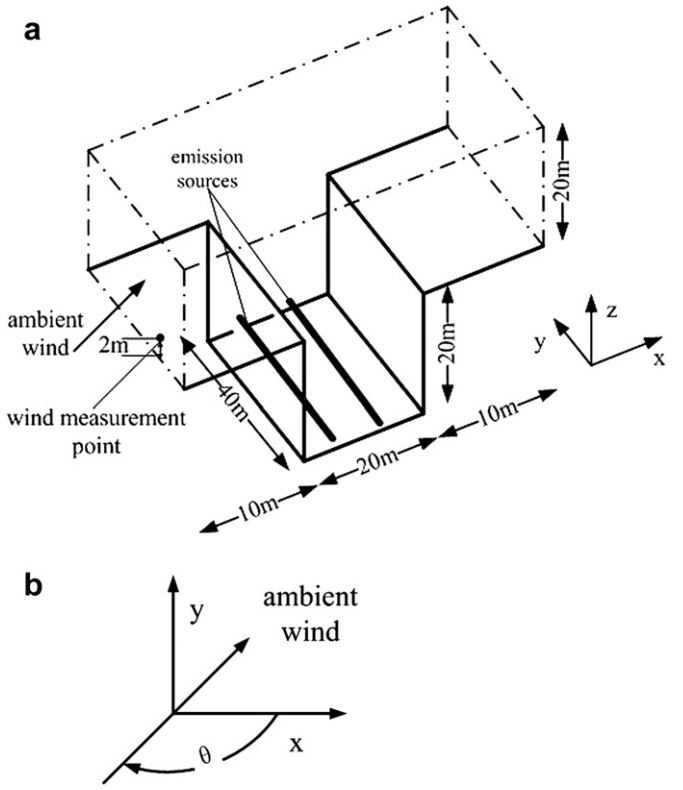

Fig. 1. Computational domain and dimensions. (a) Street canyon geometry; (b) incidence angle (θ) in the horizontal plane.

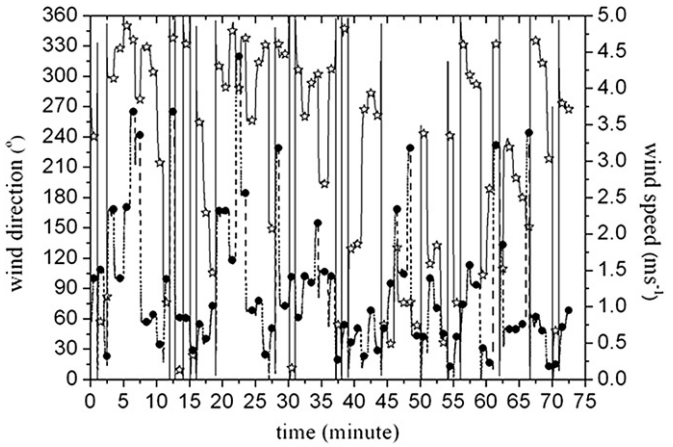

Fig. 2. The measured series of wind velocities and directions (1-min average). Stars are measured wind directions; circles are measured wind velocities.

The air flow above the roof level in the computational domain can be regarded as the local air flow since the computational domain is set as a basic element within the urban roughness sublayer (Rotach et al., 2005), which is affected by both the ambient air flow and the feedback of the air flow inside the street canyon. However, the change of ambient air flow is the triggering factor on the local air flow above the street canyon. The feedback of the air flow inside the street canyon, which is regarded as an internal source, can be calculated since it exists inside the computational domain. The effect of ambient air flow variations on the local air flow above the roof level, which is regarded as an external momentum source, can be modeled.

In the following, only horizontal wind velocities are focused on the upper boundary of street air flow for LES. The horizontal wind velocities and directions at 2 m level above a building roof in Yu Chau Street, Kowlong, Hong Kong was measured on 11 May, 2009, from 19:16 to 21:30 by a 2-D wind sonic, with data logged per minute (Zhang et al., 2011). The measured wind velocities and directions in the first 73 min are used in the simulation since these data are long enough for the analysis of the effect of RTBC on the evolution of the air flow in the street canyon. As shown in Fig. 2, these measured wind velocities and directions (at incidence angles) are denoted as U_k and θ_k, where the indices k, ranging from 1 to 73, refers to the minute series of measurement.

The time scale of the wind data measurement, hereafter noted as TSM_k, is 1 min. These measured wind data indicate the statistical averages of wind velocities and directions in each TSM_k on the measurement point (Fig. 1(a)). This means that the change of the upper boundary wind conditions should be finished in 1 min and that in the meantime the simulated flow should reach the quasi-steady flow in 1 min and reflects the average induced flow in statistics. In our scheme, the external momentum source term above the roof level is realized by the additional momentum source term, S_i, in Equation (2). For each TSM_k, the resorting of additional momentum source term to Equation (2) is done every time step, 0.4s in this work, till the upper boundary wind conditions reach the measured data in TSM_{k+1}. Then, the LES is to get the quasi-steady flow in TSM_{k+1}.

The ambient wind velocity profile above the roof level is commonly considered in the vertical exponential distribution (Klein and Plate, 1999; Pavageau and Schatzmann, 1999; Baik et al., 2000). The additional momentum source is supposed in exponential distribution and described as

$$S_{k,1}(z) = \varphi(U_k\cos(180-\theta_k)-\overline{u}_1)\left(\frac{z-H}{z_{ref}}\right)^{0.299}/\Delta t \quad (4)$$

$$S_{k,2}(z) = \varphi(U_k\sin(180-\theta_k)-\overline{u}_2)\left(\frac{z-H}{z_{ref}}\right)^{0.299}/\Delta t \quad (5)$$

where $S_{k,1}(z)$ and $S_{k,2}$ are the additional momentum source terms of the $\overline{u}_1$ and $\overline{u}_2$ momentum equations (Equation (2)), $\overline{u}_1$ and $\overline{u}_2$ are components of the resolved wind velocities in the last time step, z is the height from the ground of the current control volume center, H is the building height, $z_{ref} = 2$m is the height of measurement point to the building roof and φ is a relaxation factor. To keep the convergence of the numerical method, the value of φ is set to be 0.02 in the current work. $U_{k+1}\cos(180-\theta_{k+1})$ and $U_{k+1}\sin(180-\theta_{k+1})$ indicate the components of the measured wind velocities in the x and y directions in TSM_{k+1}, respectively, as shown in Fig. 1(b).

Fig. 3 shows the transient air flow structures inside and above the street canyon from TSM_{32} to TSM_{33}, on the middle cross section (MCS) of the canyon in the spanwise direction. The evolution of the upper boundary wind conditions is depicted in Fig. 4. Fig. 3 illustrates that a flow pattern transformation occurs with the variation of the upper boundary wind condition. The air flow structures inside and above the street canyon vary with the upper boundary wind condition in the first 0.6 min and then the flow reaches the quasi-steady condition in the last 0.4 min. It follows that the flow structures inside and above the street canyon at TSM_{k+1} can reflect the average induced flow in statistics when the upper boundary wind condition change from TSM_k to TSM_{k+1}. Note that the variation of the upper boundary wind condition from TSM_k to TSM_{k+1} on the measurement point is finished in the first 0.4 min, as shown in

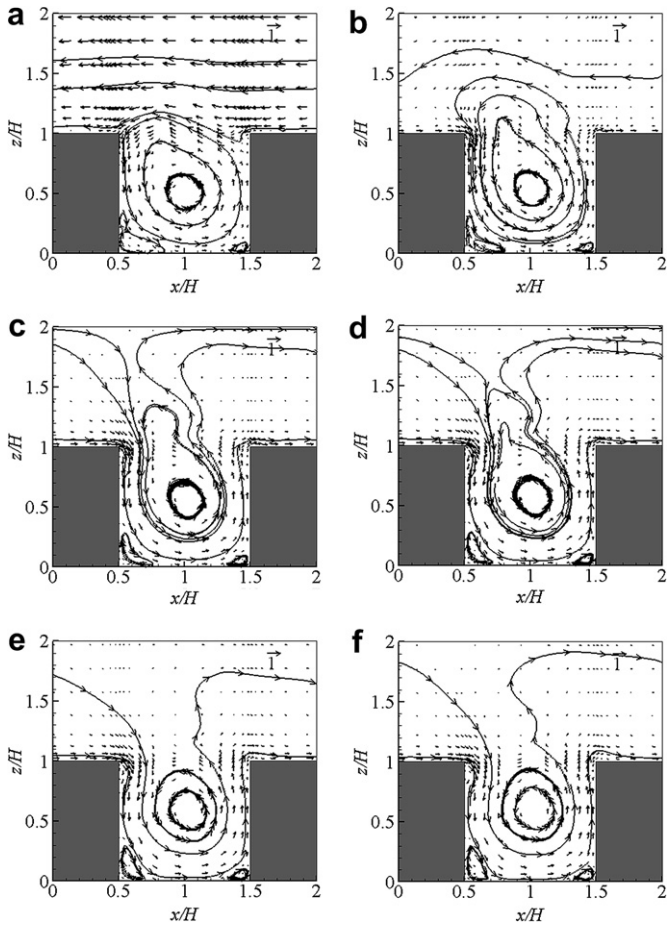

Fig. 3. Simulated transient air flow structures on the middle cross section (MCS) of the canyon in the spanwise direction from TSM_{32} to TSM_{33}. (a) t = 32.0 min, (b) t = 32.2 min, (c) t = 32.4 min, (d) t = 32.6 min, (e) t = 32.8 min, (f) t = 33.0 min.

Fig. 4, which means the flow pattern transformation has a delay. This delay is due to the effect of the feedback of the air flow inside the street canyon on the whole flow field structure.

The measured wind data are usually the mean wind conditions at each TSM_k. From the viewpoint of fluid dynamics, the change of upper boundary wind conditions from TSM_k to TSM_{k+1} is a continuous change. Our results show that the continuous change of upper boundary wind conditions has an effect on the simulated transient air flow structures inside and above the street canyon. The quasi-steady air flow structure is the consequence of the mean wind conditions at each TSM_{k+1}. The time span of the variation of upper boundary wind conditions from TSM_k to TSM_{k+1} is related to the relaxation factor, φ, which is set to be 0.02 in the current simulation. The larger the relaxation factor, the shorter the time span of adjusting the upper boundary wind conditions from TSM_k to TSM_{k+1}.

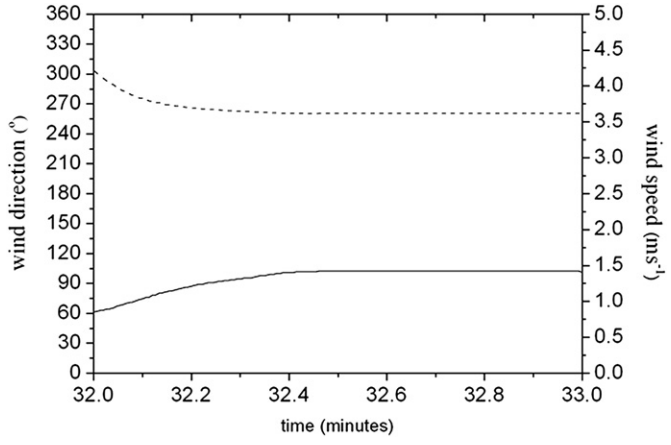

Fig. 4. The variation of upper boundary wind velocity and direction from TSM_{32} to TSM_{33}. Solid line is the wind velocity; dash line is the wind direction.

In the following, the quasi-steady air flow at each TSM_{k+1} is adopted to discuss the induced effects of time series of real-time ambient wind conditions.

4. Simulated air flow and pollutant dispersion under real-time boundary wind conditions

The air flows and pollutant dispersion inside and above the street canyon under real-time boundary wind conditions are simulated for 73 min by using the scheme described in Section 3. The air flow structures and pollutant distributions on the MCS in the spanwise direction of the canyon at several typical TSM_{k+1} are selected to demonstrate the effects of real-time boundary wind conditions on the air flows and pollutant dispersion inside and above the canyon. Especially, the primary air flow vortex structure and the position of the shear layer, which are induced by the change in the upper boundary conditions from TSM_k to TSM_{k+1}, are described to reveal the mechanism underlying the expansion and compression of the air mass in the street canyon.

4.1. Air flow structures inside and above the street canyon

Fig. 5 shows the evolution of the air flow structures inside and above the street canyon on the MCS in the spanwise direction of the canyon under RTBC. Primary vortices are built up sometime in the evolution (i.e., TSM_{30}, TSM_{35}, TSM_{45}, and TSM_{50}). A primary vortex is a typical structure inside the street canyon with SBC (given mean wind velocity and the prevailing wind direction) (Baik et al., 2000; Chan et al., 2001; Walton and Cheng, 2002; Gu et al., 2010).

Although, in this study, the RTBC experience changes in wind velocity and direction, the real-time upper boundary wind still has a prevailing wind direction of 320°(nearly perpendicular to the street canyon, see Fig. 2). Thus the basic air flow structures obtained in simulations under SBC are always found in the current simulations, even under RTBC. Nevertheless, Fig. 5 shows that primary vortex strength in the street canyon under RTBC experience highly intermittent processes.

The air flow in the street canyon with a large upper boundary wind velocity is in a regular structure with a primary vortex, as shown in the cases of TSM_{30}, TSM_{35}, TSM_{45}, and TSM_{50} in Fig. 5. However, in these cases, the primary vortex structures in the street canyon are slight different, probably because the air flow structure at TSM_{k+1} is the consequence of the variation of the upper boundary wind conditions changes from TSM_k to TSM_{k+1}, as shown in Fig. 3. In the cases of TSM_{30} and TSM_{45}, the upper boundary wind conditions change moderately, compared to those of TSM_{29} and TSM_{44} (Fig. 2). Consequently, the primary vortices are fully inside the street canyon in these cases. In the case of TSM_{35}, the upper boundary wind velocity increases considerable, when compared with that of TSM_{34} (Fig. 2); as a result, the overshoot of the upper boundary air flow leads to the compression of the primary vortex below the roof level. In the case of TSM_{50}, the upper boundary wind velocity decreases evidently, when compared with that of TSM_{49} (Fig. 2), and the decay of the upper boundary air flow results in the expansion of the primary vortex above the roof level.

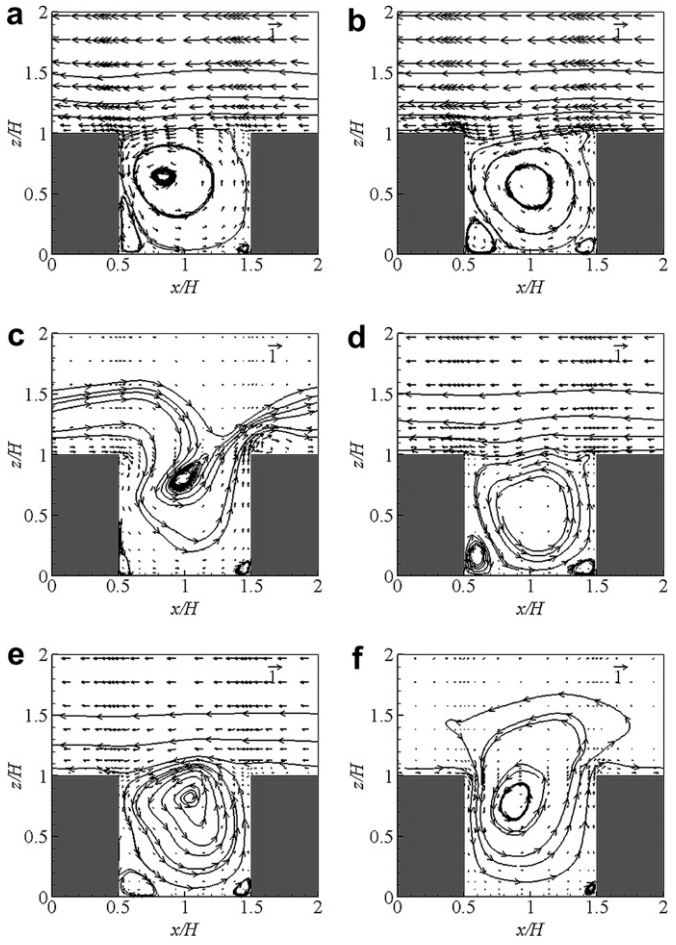

Fig. 5. Simulated wind vectors and stream lines inside and above the street canyon on MCS in the spanwise direction of the street canyon under real-time boundary conditions. (a) TSM_{30}, (b) TSM_{35}, (c) TSM_{40}, (d) TSM_{45}, (e) TSM_{50}, (f) TSM_{60}.

In the case of TSM_{60}, the upper boundary wind velocity nearly decreases to zero. In this case, the primary vortex expands considerably and occupies part of the upper boundary domain. It means that in this case, the feedback of the air flow inside the street canyon is the main factor affecting the air flow structures inside and above the canyon. The case of TSM_{40} shows the air flow structures inside and above the street canyon results from the considerable change in the boundary wind direction ($U_{39} = 0.75$ m s^{-1}, $\theta_{39} = 346.99°$, $U_{40} = 0.51$ m s^{-1} and $\theta_{40} = 129.14°$). The primary vortex is not found in the street canyon; instead, the upper boundary air flow moves downward and passes through the street canyon.

The primary vortex of the air flow inside the street canyon is commonly induced by the shear layer near the roof level (Louka et al., 2000). Physically, this shear layer is located on top of the primary vortex. The expansion or compression of the air mass in the street canyon, which results from the change in the upper boundary air flow during TSM_k and TSM_{k+1}, reflects the flapping of the shear layer. Louka et al. (2000) performed field measurements and reported the flapping of the shear layer under RTBC. However, the detachment of the shear layer in the cases of TSM_{40} and TSM_{60} was not mentioned by Louka et al. (2000).

Illustrated by the resolved scale velocities (or large scale air movement), the expansion of the primary vortex physically reveals the expansion of the air mass in the street canyon, which enhances the transport of pollutants from the canyon to the air flow above the roof level. On the other hand, the compression of the primary vortex in the street canyon physically reveals the compression of the air mass inside the canyon, which depresses the transport of pollutants from the canyon to the air flow above the roof level. The finding of the expansion or compression of the primary vortex (air mass) in the street canyon is of vital importance since this expansion or compression process is a large scale air movement and has highly significant effect on the transport of pollutants from the canyon to the upper air flow. It follows that under RTBC, the transport of pollutants from the canyon to the upper air flow are brought about by both the expansion or compression of the air mass in the street canyon and the shear layer turbulence.

In order to show the total effect of RTBC on the mean air flow structures inside and above the street canyon, the simulation of the air flow in the street canyon under SBC is conducted for 73 min. The mean wind velocity and the prevailing wind direction for the simulation are adopted from the measured wind data in the first 73 min. The results obtained during the 60-min RTBC and SBC simulations (from $t = 10$ min to $t = 70$) are statistically averaged, respectively. Mean stream lines and vectors are shown in Fig. 6. In the RTBC simulation, the main vortex in the canyon is clearly higher than the roof level while in the SBC simulation, the main vortex is fully confined inside the canyon. Statistically-averaged wind velocities above the roof level in the RTBC simulation are lower than those in the SBC simulation, while the statistically-averaged strength of the primary vortex inside the street canyon in the RTBC simulation is higher that in the SBC simulation (see Fig. 6). The difference between the RTBC and SBC simulation results indicates that the air flow strength inside the street canyon under given boundary wind conditions is underestimated by the SBC simulation.

4.2. Pollutant dispersion inside and above the street canyon

The evolution of pollutant concentration distributions on MCS the spanwise direction of the street canyon is shown in Fig. 7. Fig. 7 illustrates the non-uniform spatial distribution and the temporal accumulation of pollutant concentrations. Pollutant concentrations near the right (leeward) building wall are higher than that near the left (windward) building wall, as the mean wind direction is around 320°, and an anticlockwise primary vortex dominates the flow in the street canyon in most of simulation time. The pollutant concentration near the ground in the right corner in the case of TSM_{30} is around 0.3 mg m^{-3}, while the pollutant concentration near the ground in the right corner in the case of TSM_{60} is about 1.0 mg m^{-3}. The temporal accumulation of pollutant concentrations results from the low wind condition (Vardoulakis et al., 2003), as the mean wind velocity in the RTBC simulation is 1.05 m s^{-1}. The high pollutant concentrations near the ground in the right corner might also result from the neglect of vehicle and thermal effects on the air flow and pollutant dispersion in the RTBC simulation.

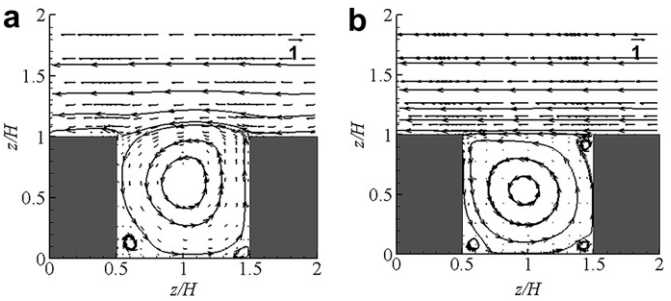

Fig. 6. Mean stream lines and vectors on MCS in the spanwise direction of the street canyon. (a) RTBC simulation; (b) SBC simulation.

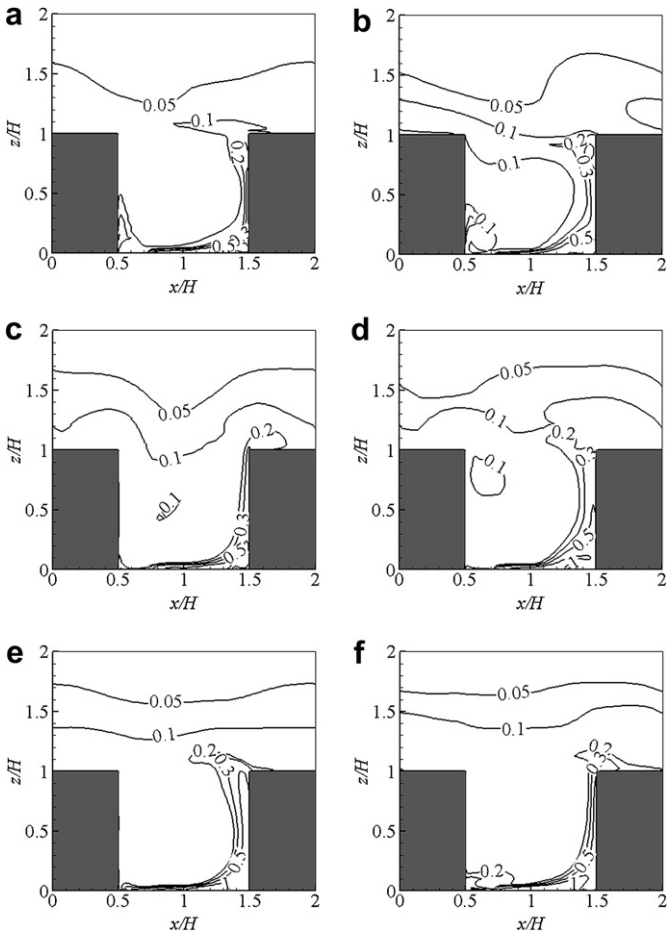

Fig. 7. Evolution of pollutant concentration (in mg m^{-3}) distribution on the MCS in the spanwise direction of the street canyon. (a) TSM_{30} (θ_{30} = 322.00°), (b) TSM_{35} (θ_{35} = 302.19°), (c) TSM_{40} (θ_{40} = 129.14°), (d) TSM_{45} (θ_{45} = 54.27°), (e) TSM_{50} (θ_{50} = 53.39°), (f) TSM_{60} (θ_{60} = 103.36°).

Under RTBC, pollutants inside and above the street canyon are transported by different dispersion mechanisms, relying on the time series of air flow structures. When air flow inside and above the canyon in the RTBC simulation has the same basic structure, as the flows in SBC simulation, that is, the flows have a primary vortex in the canyon, pollutants are transported to the roof level along the leeward wall, and then transported to the windward wall near the roof level with the primary vortex in the canyon, as shown in the cases of TSM_{30}, TSM_{35}, TSM_{45}, and TSM_{50} in Fig. 7.

When the primary vortex is compressed inside the street canyon, pollutants are transported to the windward wall in lower altitude than the roof level, followed by the merging of upper pollutants into the air flow in the canyon, as shown in the case of TSM_{35}. The compression of the air mass in the street canyon depresses the pollutant dispersion. On the contrary, when the primary vortex expands above the roof level, pollutants are transported first to the area near the leeward wall above the roof level, and then transported to the windward wall in higher altitude than the roof level, as shown in the case of TSM_{50}. The transport of pollutants from the canyon air flow to the upper air flow results directly from the expansion of the air mass in the street canyon. More pollutants are transported from the canyon air flow to the upper air flow in the expansion of the air mass in street canyon in the case of TSM_{60}, where the upper boundary wind velocity nearly decreases to zero and the primary vortex occupies the upper boundary domain and affects the upper boundary air flow structure (Fig. 5). Mazzeo et al. (2007) have also found in their field measurements that the upper pollutants are transported into the canyon air flow, or the pollutants are dispersed from the canyon air flow to the upper air flow, due to the changes in the upper boundary wind conditions. Since the boundary wind directions change considerably, no primary vortex is found in the street canyon in the case of TSM_{40}, and pollutants are transported directly by the upper boundary air flow passing by the street canyon along the leeward wall, without re-circulation in the street canyon. All the cases of TSM_{35}, TSM_{50}, TSM_{60} and TSM_{40} show the effects of the large scale air movement of the air mass in the street canyon on pollutant dispersion.

The statistically-averaged pollutant concentrations and the vertical pollutant turbulence transport fluxes during the 60 min from t = 10.0 to t = 70.0 in the RTBC simulation and the SBC simulation are studied, respectively, to demonstrate the effects of the boundary wind conditions on pollutant dispersion. Fig. 8 shows the statistically-averaged pollutant concentration distributions. As the mean air flow in the street canyon is dominated by an anticlockwise vortex (see Fig. 6). The statistically-averaged pollutant concentrations near the right wall are higher than that near the left wall in both the RTBC and the SBC simulations, which is in accordance with common sense. Pollutant concentrations in areas inside the street canyon and near the roof level in the RTBC simulation are lower than those in the SBC simulation; however, the pollutant concentration far above the roof level in the RTBC simulation is higher than that in the SBC simulation. In the SBC simulation, mean pollutant concentration distributions are only affected by the air vortex in the street canyon, with mean pollutant concentration contours extending to the windward wall at the roof level. The RTBC often cause the large scale air movement of the air mass in the street canyon (i.e., the expansion or compression processes of the air mass in the street canyon), enhancing the pollutant dispersion. Therefore, in the RTBC simulation, the mean pollutant concentration contours extend from the roof level to the upper boundary domain near the leeward wall. It proves that the RTBC produce better conditions for the pollutant dispersion than the artificially-designed SBC.

Fig. 9 shows the contours of the vertical pollutant turbulence transport fluxes. In the SBC simulation, the vertical pollutant turbulence transport flux has large positive values at the roof level and near the windward wall, but negative values near the leeward wall, which has been proved by previous studies (Walton and Cheng, 2002; Zhang et al., 2011). Walton et al. (2002) also found that the transport of pollutants from the street canyon to the upper layer mainly happens near the windward wall at the roof level, as the transport is mainly affected by the shear layer turbulence or by the Kelvin–Helmholtz instability. In the RTBC simulation, the vertical pollutant turbulence transport flux has large positive values near the leeward wall and near the windward wall, but low

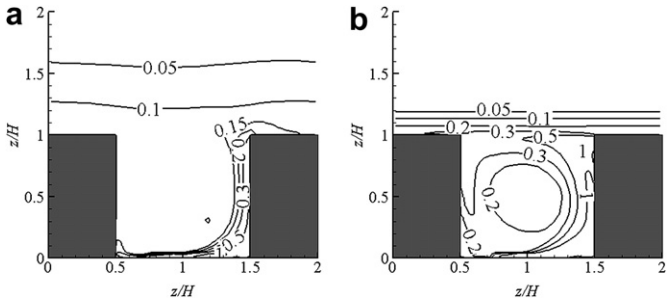

Fig. 8. Contours of statistically-averaged pollutant concentrations, mg m^{-3}. (a) RTBC simulation; (b) SBC simulation.

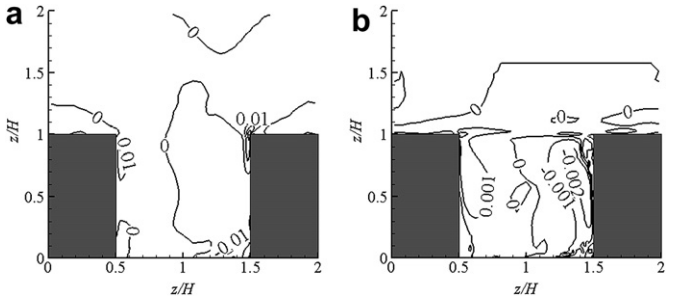

Fig. 9. Contours of vertical pollutant turbulence transport fluxes ($u_3'c'$), mg m^{-2} s^{-1}. (a) RTBC simulation; (b) SBC simulation.

positive values in the center of the roof level. The distribution of the vertical pollutant turbulence transport flux indicates that the turbulence affecting the pollutant transport at the roof level may be not from the Kelvin–Helmholtz instability, but from the evolution of the resolved scale wind velocities as the consequence of time series of upper boundary wind condition changes. The distribution of the vertical pollutant turbulence transport flux in the RTBC simulation also indicates that the transport of pollutants from the street canyon to the upper area occurs near the leeward wall due to the expansion of the air mass in the street canyon. The expansion of the air mass in the street canyon plays a key role in the transport of pollutants from the canyon to the upper air flow under the RTBC. In addition, the values of the vertical pollutant turbulence transport flux in the RTBC simulation are generally one order of magnitude higher than those in the SBC simulation, suggesting that the SBC simulation has underestimated the real-time air flow turbulence inside and above the canyon.

5. Conclusions

For a large eddy simulation of air flow in a street canyon, it is important to use time series of boundary wind conditions as inputs. The basic air flow structures obtained in simulations under the SBC are still found in the current simulations as the real-time upper boundary wind has a prevailing wind direction (320°) that nearly perpendicular to the street canyon. Nevertheless, the air flow structure in the street canyon and the strength of the primary vortex under RTBC experience highly intermittent processes. Due to the variations of the upper boundary wind conditions, the expansion or compression of the primary vortex (air mass) in the street canyon is a large scale air movement of the air mass and has a highly significant effect on the transport of pollutants from the canyon to the upper air flow.

Under RTBC, pollutants inside and above the street canyon are transported by different dispersion mechanisms, relying on the time series of air flow structures. When the air flows inside and above the canyon in the RTBC simulation have the same basic structure as the flows in the SBC simulation, that is, the flows have a primary vortex in the canyon, pollutants are transported to the roof level along the leeward wall, and then transported to the windward wall near the roof level with the primary vortex. However, the RTBC often cause large scale air movement of air mass in the street canyon (the expansion or compression processes of the air mass in the street canyon), enhancing the pollutant dispersion. The distribution of the vertical pollutant turbulence transport flux also indicates that the turbulence affecting the pollutant transport at the roof level may be not from the Kelvin–Helmholtz instability, but from the evolution of the resolved scale wind velocities as the consequence of time series of upper boundary wind condition changes. The values of the vertical pollutant turbulence transport flux in the RTBC simulation are generally one order of magnitude higher than those in the steady boundary condition simulation, suggesting that the steady boundary condition simulation has underestimated the real-time air flow turbulence inside and above the canyon. It follows that RTBC produce better conditions for pollutant dispersion than the artificially-designed SBC.

Acknowledgments

This study is financially supported by the National Natural Science Foundation of China (No. 10872159 & 40675011), Interdisciplinary Program of Xian Jiaotong University (2009xjtujc10).

References

Baik, J.J., Park, R.S., Chun, H.Y., Kim, J.J., 2000. A laboratory model of urban street-canyon flows. Journal of Applied Meteorology 39 (9), 1592–1600.
Cai, X.M., Barlow, J.F., Belcher, S.E., 2008. Dispersion and transfer of passive scalars in and above street canyons – large-eddy simulations. Atmospheric Environment 42, 5885–5895.
Chan, A.T., So, E.S.P., Samad, S.C., 2001. Strategic guidelines for street canyon geometry to achieve sustainable street air quality. Atmospheric Environment 35 (24), 4089–4098.
Cooke, R.M., Wilson, A.M., Tuomisto, J.T., Morales, O., Tainio, M., Evans, J., 2007. A probabilistic characterization of the relationship between fine particulate matter and mortality: elicitation of European experts. Environment Science and Technology 41 (18), 6598–6605.
Cui, Z.Q., Cai, X.M., Baker, C.J., 2004. Large-eddy simulation of turbulent flow in a street canyon. Quarterly Journal of the Royal Meteorological Society 130 (599), 1373–1394.
Depaul, F.T., Sheih, C.M., 1985. A tracer study of dispersion in an urban street canyon. Atmospheric Environment 19 (4), 555–559.
Eliasson, I., Offerle, B., Grimmond, C.S.B., Lindqvist, S., 2006. Wind fields and turbulence statistics in an urban street canyon. Atmospheric Environment 40 (1), 1–16.
Fenger, J., 1999. Urban air quality. Atmospheric Environment 33 (29), 4877–4900.
Gromke, C., Ruck, B., 2007. Influence of trees on the dispersion of pollutants in an urban street canyon – experimental investigation of the flow and concentration field. Atmospheric Environment 41 (16), 3287–3302.
Gu, Z.L., Zhang, Y.W., Lei, K.B., 2010. Large eddy simulation of flow in a street canyon with tree planting under various atmospheric instability conditions. Science China – Technological Sciences 53 (7), 1928–1937.
Hoydysh, W.G., Dabberdt, W.E., 1988. Kinetics and dispersion characteristics of flows in asymmetric street canyons. Atmospheric Environment 22, 2677–2689.
Kim, J.J., Baik, J.J., 2001. Urban street-canyon flows with bottom heating. Atmospheric Environment 35 (20), 3395–3404.
Klein, P.K., Plate, E.J., 1999. Wind-tunnel study of concentration fields in street canyons. Atmospheric Environment 33, 3373–3979.
Li, X.X., Liu, C.H., Leung, D.Y.C., 2008. Large-eddy simulation of flow and pollutant dispersion in high-aspect-ratio urban street canyons with wall model. Boundary-Layer Meteorology 129, 249–268.
Li, X.X., Liu, C.H., Leung, D.Y.C., 2009. Numerical investigation of pollutant transport characteristics inside deep urban street canyons. Atmospheric Environment 43, 2410–2418.
Liu, C.H., Barth, M.C., 2002. Large-eddy simulation of flow and scalar transport in a modeled street canyon. Journal of Applied Meteorology 41 (6), 660–673.
Louka, P., Belcher, S.E., Harrison, R.G., 2000. Coupling between air flow in streets and the well-developed boundary layer aloft. Atmospheric Environment 34 (16), 2613–2621.
Mazzeo, N.A., Venegas, L.E., Martin, P.B., 2007. Analysis of full-scale data obtained in a street canyon. Atmosfera 20 (1), 93–110.
Murena, F., Favale, G., Vardoulakis, S., Solazzo, E., 2009. Modelling dispersion of traffic pollution in a deep street canyon: application of CFD and operational models. Atmospheric Environment 43 (14), 2303–2311.
Pavageau, M., Schatzmann, M., 1999. Wind tunnel measurements of concentration fluctuations in an urban street canyon. Atmospheric Environment 33 (24–25), 3961–3971.
Qiu, J., Gu, Z.L., Wang, Z.S., 2008. Numerical study of the response of an atmospheric surface layer to a spatially nonuniform plant canopy. Boundary-Layer Meteorology 127, 293–311.
Rotach, M.W., 1995. Profiles of turbulence statistics in and above an urban street canyon. Atmospheric Environment 29 (13), 1473–1486.
Rotach, M.W., Vogt, R., Bernhofer, C., Batchvarova, E., Christen, A., Clappier, A., Feddersen, B., Gryning, S.E., Martucci, G., Mayer, H., Mitev, V., Oke, T.R., Parlow, E., Richner, H., Roth, M., Roulet, Y.A., Ruffieux, D., Salmond, J.A., Schatzmann, M., Voogt, J.A., 2005. BUBBLE – an urban boundary layer meteorology project. Theoretical and Applied Climatology 81 (3), 231–261.
Smagorinsky, J., 1963. General circulation experiments with the primitive equations: part 1. The basic experiment. Monthly Weather Review 91, 99–164.
Tao, W.Q., 2005. Recent Advancement in Numerical Heat Transfer. Science Press, Bei Jing, pp. 125–131.

Vardoulakis, S., Fisher, B.E.A., Pericleous, K., Gonzalez-Flesca, N., 2003. Modelling air quality in street canyons: a review. Atmospheric Environment 37 (2), 155–182.

Walton, A., Cheng, A.Y.S., 2002. Large-eddy simulation of pollution dispersion in an urban street canyon – part II: idealised canyon simulation. Atmospheric Environment 36 (22), 3615–3627.

Walton, A., Cheng, A.Y.S., Yeung, W.C., 2002. Large-eddy simulation of pollution dispersion in an urban street canyon – part I: comparison with field data. Atmospheric Environment 36 (22), 3601–3613.

WHO, 2006. Air Quality Guidelines for Particulate Matter, Ozone Nitrogen, Dioxide and Sulfur Dioxide, Global Update 2005, Summary of Risk Assessment. World Health Organization, Geneva, Switzerland.

Yang, Y., Shao, Y., 2008. Numerical simulations of flow and pollutant dispersion in urban atmospheric boundary layers. Environmental Modeling & Assessment 23, 906–921.

Zhang, Y.W., Gu, Z.L., Lee, S.C., Fu, T.M., Ho, K.F., 2011. Numerical simulation and in situ investigation of fine particle dispersion in an actual deep street canyon in Hong Kong. Indoor and Built Environment. doi:10.1177/1420326X10387694.